LAWRENCE
LIVERMORE
NATIONAL
LABORATORY

LLNL-JRNL-421685

Observation of Strong Resonant Behavior in the Inverse Photoelectron Spectroscopy of Ce Oxide

J.G. Tobin, S-W Yu, B.W. Chung, G.D. Waddill, E. Damian, L. Duda, J Nordgren

December 21, 2009

Physical Review B

Disclaimer

Observation of Strong Resonant Behavior in the Inverse Photoelectron Spectroscopy of Ce Oxide

J.G. Tobin*[,1], S.W. Yu[1], B.W. Chung[1], G.D. Waddill[2],
E. Damian[3], L. Duda[3] and J. Nordgren[3]

1. Lawrence Livermore National Laboratory, Livermore, CA, USA
2. Missouri University of Science and Technology, Rolla, MO. USA
3. Uppsala University, Uppsala, Sweden
*Contact Author: Tobin1@LLNL.Gov

Abstract

X-ray Emission Spectroscopy (XES) and Resonant Inverse Photoelectron Spectroscopy (RIPES) have been used to investigate the photon emission associated with the $Ce3d_{5/2}$ and $Ce3d_{3/2}$ thresholds. Strong resonant behavior has been observed in the RIPES of Ce Oxide near the 5/2 and 3/2 edges.

I Introduction

Inverse Photoelectron Spectroscopy (IPES) and its high energy variant, Bremstrahlung Isochromat Spectroscopy (BIS), are powerful techniques that permit a direct interrogation of the low-lying unoccupied electronic structure of a variety of materials. Despite being handicapped by counting rates that are approximately four orders of magnitude less that the corresponding electron spectroscopies (Photoelectron Spectroscopy, PES, and X-ray Photoelectron Spectroscopy, XPS) both IPES [1,2,3,4,5] and BIS [6,7,8] have a long history of important contributions. Over time, an additional variant of this technique has appeared, where the kinetic energy (KE) of the incoming electron and photon energy (hv) of the emitted electron are roughly the same magnitude as the binding energy of a core level of the material in question. Under these

circumstances and in analogy to Resonant Photoelectron Spectroscopy, a cross section resonance can occur, giving rise to Resonant Inverse Photoelectron Spectroscopy or RIPES. [9-13] Here, we report the observation of RIPES in an f electron system, specifically the at the $3d_{5/2}$ and $3d_{3/2}$ thresholds of Ce Oxide. (Please see Figure 1.)

The resonant behavior of the Ce4f structure at the 3d thresholds has been addressed before, including studies of the utilization of the technique as a probe of electron correlation in a variety of Ce compounds. [12] Interestingly, the first RIPES work on rare earths dates back to 1974, although under conditions which left the state of the surface and near surface regions undefined. Although they did not use the more modern terminology of "RIPES," it is clear that RIPES was actually first performed in 1974 by Liefeld, Burr and Chamberlain on both La and Ce based materials. [9] In these experiments, the La and Ce metallic samples were attached to the anode of an x-ray tube and the x-ray emission characteristics were measured using a two crystal monochromator. The pressure in the x-ray tube was quoted as being below 2×10^{-8} Torr. They did indeed observed resonant behavior at the Mα ($3d_{5/2}$) and Mβ ($3d_{3/2}$) thresholds. In fact, our results here will confirm the measurements made upon the Ce based sample used in by Liefeld et al. However, the state of the Ce sample surface and near surface regions are quite undefined in the study in Ref 9. For example, the authors suggest that they are probing Ce metal, since they cannot see any evidence of an OKα (1s) XES line. However, they do report the observation of FKα (1s) line, possibly due to the utilization of cerium fluoride in the sample

preparation. Later, they tried to address these issues in a new ultrahigh vacuum system. [13] Based upon our results, it is clear that their original sample surface was oxidized, using the word here in its more general context as in having lost electrons to the oxidizing agent, although whether the structure is an oxide or fluoride remains unclear. In any case, the primacy of Liefeld and coworkers in these measurements should be noted.

Cerium and cerium oxide have been studied with a variety of spectroscopic techniques under UHV conditions. This includes Bremstrahlung Isochromat Spectroscopy or BIS [6], Photoelectron Spectroscopy [6, 14- 18], X-ray Absorption Spectroscopy[19, 20, 21], Electron Energy Loss Spectroscopy [6,20, 22,23] and Resonant XES [24,25], to name just a few. We will compare our results to those of other spectroscopies, as will be discussed below.

The remainder of this paper will be as follows. In Section II, the experimental details will be briefly described. In Section III, the determination of sample quality with XES and the RIPES results will each be presented and discussed, within the context of the mechanisms of RIPES and XES, as shown in Figure 2. Finally, Section IV will contain a Summary and Conclusions.

II Experimental

The experiments were carried out onsite at Lawrence Livermore National Laboratory, using a spectrometer [26] with capabilities for performing both spin resolved Fano spectroscopy [27] and high energy Inverse Photoelectron Spectroscopy (IPES) or Bremstrahlung Isochromat Spectroscopy (BIS). [28] The XES and IPES/BIS spectra were collected using a Specs electron gun for the

excitation and the XES 350 grating monochromator and channel plate system from Scienta as the photon detection. Spectra were collected in "normal mode," where the electron gun kinetic energy (KE) and the energy position of the center of the channel plate were both fixed and the energy distribution in the photon (hv) spectrum was derived from the intensities distributed across the channel plate detector in the energy dispersal direction. The polycrystalline Ce sample was oxidized by exposure to air at ambient pressures. After introduction to the ultra-high vacuum system, the oxidized sample was bombarded with Ar ions and underwent annealing, to clean the topmost surface region and stabilize the surface and near surface regions. XES and RIPES data collection occurred with the sample at or near room temperature. In our experiments, the XES spectra play two critical roles: (1) the definition of the energy scale and location of the resonance in energy space for RIPES and (2) the confirmation of the sample quality. Topic 2 will be discussed below. For the energy scale, the calibration was based upon assigning the literature values [27] for the peaks at the Ce Mα ($3d_{5/2}$) and Mβ ($3d_{3/2}$) thresholds, as shown in Figure 1. While the internal calibration of the monochromator provides energy positions that are close to the correct values, a final adjustment is necessary, corresponding to $\Delta\lambda$ = 0.4 angstroms. A similar shift was applied to the O1s spectra, with the appropriate scaling with the photon energy squared. As shown in Figure two, the underlying energy conservation relationship for IPES/BIS is hv + H^F is equal to KE + ϕ, where hv is the photon energy, H^F is the energy of the empty state (hole) filled, relative to the Fermi Energy (E_F), KE is the Kinetic Energy of the incoming

electron and ϕ is some sort of work function. Because the KE used here is from the output of the electron gun system, ϕ is a spectrometer work function and can contain contact potentials and other offsets. In the case of our spectrometer, the spectrometer work function, ϕ_{sp}, is approximately 9 volts. The base pressure of the system was 3×10^{-10} torr, but the pressure changed depending the energy and current of the electron gun. For example, with the XES measurements at KE =3KeV, the pressure was approximately 8 to 9 $x10^{-10}$ torr and the excitation current to the sample was typically 0.01 mA , but for RIPES at KE of approximately 900 eV, it was about $5x10^{-10}$ torr and 0.003 mA. XES data collection was fairly quick but RIPES spectra required many hours each. The energy resolution bandpass in the experiment was driven by the broadening contributions of the electron gun and photon detection, which in turn is dependent upon the slit widths chosen for the monochromator. Using the 90%-10% width of the Fermi Edge (E_F), it is possible to determine directly the total energy bandpass in the RIPES experiments. As will be discussed below, our sample consisted of a thin layer of Ce Oxide lying above Ce metal. Under conditions such as these, thin layers composed of materials that would normally be insulating in the bulk can continue to exhibit a Fermi edge, owing to the thinness of the film and the underlying conductor. [28] It is for this reason that we will refer to the sample as Ce Oxide. Although thermodynamic arguments all point to CeO_2, the absence of a band gap and the thinness of the sample militate for a more generic moniker. Because the total energy bandpass is on the order of eV's, the intrinsic, temperature dependent broadening of the Fermi Edge

caused by Fermi statistics can be neglected. An experimental bandpass of approximately 2eV was found for all of the monochromator slit sizes used. An example of this is shown in Figure 1. The independence of the energy bandpass from the slit size suggests that the energy bandpass is dominated by the contribution from the electron gun, with a value near 2 eV. Despite the apparent lack of dependence upon slit size, for some measurements slit sizes were varied, as a test of data set consistency.

III Spectral Results and Discussion

IIIa Confirmation of Sample Quality

XES of the Ce $3d_{5/2}$, Ce $3d_{3/2}$ and O1s levels were used to characterize the Ce Oxide sample. As shown in Figure 1, there are two components to the Mα ($3d_{5/2}$) peak but only one for the Mβ ($3d_{3/2}$) peak. This is not surprising: the larger lifetime broadening associated with the Mβ ($3d_{3/2}$) threshold can smear out fine structure. Some of the processes involved in the production of these spectral features can be seen in Figure 2. Because $3d_{3/2}$ states are at a higher binding energy relative to the Fermi Level (B^F) than the $3d_{5/2}$ states, a fast, non-radiative decay through the $3d_{5/2}$ states is possible, contributing to the broadening. Furthermore, decay channels such as this can also explain the divergence of the peak intensities from the “statistical” limit, where intensity should scale with the number of states. In this limit, the ratio of the intensities, $3d_{5/2}$ versus $3d_{3/2}$ should be 3:2. The observed intensity ratio is quite a bit larger, as can be seen in Figure 1. Next, we will use the KE dependence of the excitation to probe the origin of the splitting in the $3d_{5/2}$ peak and relate that to the

sample structure.

As shown in Figure 3, it is possible to induce changes in the relative intensities of the two components in the Ce $3d_{5/2}$ spectral feature. These two components will be assigned to the underlying Ce metal and the near surface Ce Oxide thin film. There are two data sets shown in Figure 3, corresponding to two different slit sizes for the monochromator. In both cases, lowering the KE from 3KeV to 1.5 KeV enhances the second component of the Ce $3d_{5/2}$ spectral feature. Under these conditions, the escape depths of the photons should not be a factor, but the penetration depths of the electrons should. By lowering the KE, the surface sensitivity is increased. This argues for the material associated with the sub-peak at the lower photon energy to be underneath the material associated with the sub-peak at the higher photon energy. It is reasonable to assume that the underlying material is metallic Ce and that the layer above it is oxidized Ce. This assignment is confirmed by a consideration of the literature and previous experiments. It was shown early on by Baer and coworkers [6] that CeO_2 exhibited additional spectral structure in XPS and EELS at higher binding energies, relative to Ce metal. This result has been confirmed by others using XPS [18] and EELS [22]. Similar intensity shifts to higher energies has been observed in XAS as well. [19] In fact, as part of a previous collaboration [20], we have observed this shift before, utilizing XAS on Beamline 8 at the Advanced Light Source. [21] Using oxidized bulk Ce samples, it was possible to see strong, shifted spectral structure which could be removed by scraping, giving rise to a final XAS result which approximated the evaporated samples utilized in our other

study. [20] Thus, there is very strong evidence to support the assignment of the lower photon energy sub-peak in the Ce $3d_{5/2}$ manifold to the underlying bulk metallic Ce and the higher photon energy sub-peak to a near surface layer of CeOxide.

The above interpretation is further supported by the O1s XES data plotted in Figure 4. First, there can be no doubt that this sample is an oxide of some sort: a strong O1s spectral feature is clearly evident. Second, the result is independent of electron excitation energy, for both data sets with different slit sizes, indicating that all of the oxygen is at or near the surface, not in the bulk. Third, most of the intensity is in the main feature at a photon-energy of 525 eV. This main feature is assigned to the near surface thin film of CeOxide. The second, smaller feature near 527 eV is associated with true surface oxygen, possibly physically or chemically attached to the top of the CeOxide layer. It is reasonable to expect that the physically or chemically attached oxygen may be in a higher oxidation state, i.e. without the oxidized electrons from Ce, and would thus be at a higher photon energy. [Since oxygen is the oxidizing agent, it is the Ce that gets oxidized and the oxygen that gets reduced. A reduced atom may have less of a tight hold upon its electrons, thus giving rise to a lower binding energy. Thus the oxygen in CeOxide is expected to have a lower O1s binding energy than the physically or chemically absorbed oxygen species.]

Thus, supported by the XES results, our picture is the following. The bulk Ce is coated with a thin film of Ce Oxide, probably very much like CeO_2, but thin

enough that we see the retention of a Fermi Edge in the RIPES spectra. Next, the RIPES spectra will be described and discussed.

IIIb RIPES of the Ce 3d states

A strong resonance in the RIPES of Ce Oxide has been observed. Here, we will will present the experimental XES and RIPES data and discuss them within the framework of previous results.

As shown in Figure 1, the RIPES and XES are coincident in energy space. The difference in the spectra is due to the change in the energy of the incoming beam. For the XES, the excitation beam is at an energy of 3KeV, well above the Ce Mα ($3d_{5/2}$) and Mβ ($3d_{3/2}$) thresholds. As illustrated in Figure 2, the electron beam serves only to scatter off of the core level electrons and generate a core hole, beginning the process that ultimately gives rise to the photon emission at the characteristic energies associate with XES. Using the XES as a guide, a photon energy window was thus chosen for the RIPES experiments. As can be seen in Figure 1, the RIPES spectrum at KE = 881 eV is much sharper than the XES spectrum. Consistent with the picture shown in Figure 2, there is no intensity at the higher photon energies, above E_F. This is because the transitions in this regime would correspond to the incoming electron dropping into an occupied state, which is forbidden. The intensity jump occurs at E_F and continues into the regime where H^F is greater than zero, where the incoming electron is dropping into the unoccupied conduction band. The defining characteristic of IPES is that KE ≈ hv. For RIPES to occur, a second, indirect channel must open up, providing an additional path into the final state associated

with IPES. There are further, quantum-mechanically-driven aspects to a resonance, but that discussion can be found elsewhere. [31] Energetically, the defining characteristic of being on resonance is that KE ≈ B^F, the core level binding energy relative to the Fermi Level, E_F. Thus for RIPES, hv ≈ KE ≈ B^F, as presented schematically in Figure 2. As the photon energy diminished further, the RIPES intensity drops, as the final state moves out of the higher density conduction bands and into the less dense, more-free-electron-like states. It should also be noted that resonance effects tend to be strongest for those core level transitions following electric dipole selection rules. The strong amplification in RIPES based upon the $3d_{5/2}/3d_{3/2}$ – 4f interaction is consistent with the electric dipole selection rules.

Spectral summaries of the RIPES and XES are shown in Figures 5 -8, for the Ce $3d_{5/2}$ and Ce $3d_{3/2}$ thresholds. As can be seen in Figures 5 and 6, in both cases, it is clear that the resonance occurs only within the confines of the energy regime defined by the XES spectrum. However, to see the photon energy dependence of the resonance, it is necessary to plot each of the RIPES spectra separately, as shown in Figure 7 and 8. For the Ce $3d_{5/2}$, there appear to be weak intensities at KE = 877 and 887 eV, that suggest off-resonance spectral structure, shifting with KE. This would be the spectral dispersion of IPES driven by the linear relationship between hv and KE, as shown in Figure 2. In the intervening KE's, the resonance is dominant and the intensity reflects not so much dispersion with the changing KE but instead the onset and subsequent diminishment of a fixed peak, as it moves through resonance with a maximum at

KE = 881 eV. A similar process occurs for the Ce $3d_{3/2}$ resonance, with a maximum of the higher photon energy peak occurring at KE near 900 eV. The Ce $3d_{3/2}$ RIPES is complicated by the presence of a Ce $3d_{5/2}$ peak. This is the RIPES manifestation of the non-radiative decay process shown in Figure 2. Thus, some of the Ce $3d_{3/2}$ RIPES intensity is lost to this XES-like feature.

Now, let us return to a consideration of the RIPES versus the XES. The RIPES is shifted to lower photon energy relative to the high photon edge of the XES. It is important to remember at this point that although the final absolute energy calibration is based upon the literature values, the relative energy calibration is based upon the observation of the XES experimentally. Thus, although a re-calibration might shift the energy scale of the spectra, the relative positions of the XES and RIPES would remain fixed. Additionally, while the XES is of sufficiently high KE energy that both the near surface CeOxide and underlying Ce can be observed, with the lower KE at resonance, it is reasonable to expect that the near surface material, the CeOxide, should dominate the RIPES intensities. Thus, it appears that the resonance is associated with the CeOxide and not the metallic Ce. This interpretation is confirmed by a consideration of the results shown in Figure 9. Here, the results of measurements of metallic Ce, carried out in a similar spectrometer, are presented. [32,33] The resonance appears to be far weaker in the metallic Ce than in the CeOxide. The picture of resonance enhancement with the transition from delocalized to localized behavior is not new and this interpretation is consistent with a picture put forward earlier by Dowben. [34]

Finally, it is useful to compare our results to those of Liefeld, Burr and Chamberlain. [9] Our RIPES spectroscopic results are in essentially complete agreement with theirs. The photon energy dependences at both the Ce Mα ($3d_{5/2}$) and Mβ ($3d_{3/2}$) thresholds are same. Thus it seems very unlikely that the source of their RIPES was Ce metal, but rather is some sort of oxidized Ce, although the exact nature of the oxidation, either cerium oxide or cerium fluoride, remains unknown.

IV Summary and Conclusions

Strong resonant behavior in the Inverse Photoelectron Spectroscopy of a thin layer of CeOxide, near the Ce 3d edges, has been observed. It confirms the picture of resonance enhancement with localization and explains the observations of Liefeld, Burr and Chamberlain from 35 years ago.

Acknowledgements

Lawrence Livermore National Laboratory is operated by Lawrence Livermore National Security, LLC, for the U.S. Department of Energy, National Nuclear Security Administration under Contract DE-AC52-07NA27344. This work was supported by the DOE Office of Science, Office of Basic Energy Science, Division of Materials Science and Engineering. We would like to thank Jinghua Guo for his mentoring of ED and Jonathan Denlinger for his help with the Beamline 8 experiments at the ALS.

Observation of Strong Resonant Behavior in the Inverse Photoelectron Spectroscopy of Ce Oxide

References

1. G. Denninger, V. Dose, and H. P. Bonzel, Phys. Rev. Lett. **48**, 279 (1982); V. Dose, Appl. Phys. **14**, 117 (1977).
2. P. D. Johnson and N. V. Smith, Phys. Rev. Lett. **49**, 290 (1982).
3. F. J. Himpsel and Th. Fauster, Phys. Rev. Lett. **49**, 1583 (1982).
4. B.J. Knapp and J.G. Tobin, Phys. Rev. B **37**, 8656 (1988).
5. J.G. Tobin, "Photoemission and Inverse Photoemission," in "Determination of Optical Properties," Vol. VIII in Physical Methods of Chemistry, 2nd edition, Ed. B.W. Rossiter and R.C. Bretzold, John Wiley and Sons, New York, 1993 and references therein. E. Wuilloud, B. Delley, W.D. Schneider, and Y. Baer, Phys. Rev. Lett. **53**, 202 (1984); E. Wuilloud, H.R. Moser, W.D. Schneider, and Y. Baer, Phys. Rev. B **28**, 7354 (1983);
6. J.W. Allen, J. Magn. Mater. **47/48**, 168 (1985). check
7. P. Kuiper, J. van Elp, G.A. Sawatzky, A. Fujimori, S. Hosoya, and D.M. de Leeuw, Phys. Rev. B **44**, 4570 (1991).
8. R. J. Liefeld, A.F. Burr and M.B. Chamberlian, Phys. Rev. A **9**, 316 (1974); M.B. Chamberlain, A.F. Burr, and R.J. Liefeld, Phys. Rev. A **9**, 663(1974).
9. F. Reihle, Phys. Status Solidi **98**, 245 (1980).
10. Y.Hu, T.J. Wagener, Y. Gao, J.H. Weaver, Phys. Rev B **38**, 12709 (1988).
11. P. Weibel, M. Grioni, D. Malterre, B. Dardel, and Y. Baer, Phys. Rev. Lett. **72**, 1252 (1994); M. Grioni, P. Weibel, D. Malterre, Y. Baer, and L. Du`o, Phys. Rev. B **55**, 2056 (1997).
12. B.E. Mason, R.J. Liefeld, J. Vac. Sci. Tech. A **8**, 4057 (1990).

13. D. Wieliczka, J. H. Weaver, D. W. Lynch, and C. G. Olson, Phys. Rev. B **26**, 7056 (1982)
14. E. Vescovo and C. Carbone, Phys. Rev. B **53**, 4142 (1996).
15. E. Weschke, C. Laubschat, T. Simmons, M. Domke, O. Strebel, and G. Kaindl, Phys. Rev. B. **44**, 8304 (1991).
16. P. Pasala, S. Logothetidis, L. Sygellou and S, Kennou, Phys. Rev. B **68**, 035104 (2003).
17. N.A. Braaten, J.K. Grepstad, and S. Raaen, Phys. Rev. B **40**, 7969 (1989).
18. C. Bonnelle, R.C. Karnatak, and J. Sugar, Phys. Rev. A **9**, 1920 (1974).
19. K.T. Moore, B.W. Chung, S.A. Morton, S. Lazar, F.D. Tichelaar, H.W. Zandbergen, P. Söderlind, G. van der Laan, A.J. Schwartz, and J.G. Tobin, Phys. Rev. B **69**, 193104 (2004).
20. J. Denlinger, private communication, December 2009.
21. J. Bloch, N. Shamir, M.H. Mintz and U. Atzmony, Phys. Rev. B. **30**, 2462 (1984).
22. Lijun Wu, H.J. Wiesmann, A.R. Moodenbaugh, R.F. Klie, Yimei Zhu, D.O. Welch and M. Suenaga, Phys. Rev. B **69**, 125415 (2004).
23. C. Dallera, M. Grioni, A. Palenzona, M. Taguchi, E. Annese, G. Ghiringhelli, A. Tagliaferri, N. B. Brookes, Th. Neisius, and L. Braicovich, Phys. Ev. B **70**, 085112 (2004).
24. M. Watanabe, Y. Harada, M. Nakazawa, Y. Oshiwata, R. Eguchi, T. Takeuchi, A. Kotani and S. Shin, Surf. Rev. Lett. **9**, 983 (2002).
25. J.G. Tobin, S.W. Yu, T. Komesu, B.W. Chung, S.A. Morton, and G.D.

Waddill,Matl. Res. Soc. Symp. Proc. **986**, 63 (2007).

26. S.W. Yu and J. G. Tobin, Phys. Rev. B **77**, 193409 (2008); S.W. Yu and J.G. Tobin, Surface Science Letters **601**, L127 (2007).
27. J.G. Tobin, S.-W. Yu, B.W. Chung, G.D. Waddill and AL Kutepov, "Narrowing the Range of Possible Solutions to the Pu Electronic Structure Problem: Developing a new Bremstrahlung Isochromat Spectroscopy Capability," IOP Conference Series, Materials Science and Engineering, Actinides 2009 International Meeting, San Francisco, CA, USA, July 12-17, 2009.
28. X-ray Data Handbook, A. Thompson et al, LBNL, Berkeley, CA,USA, Jan 2001.
29. B.W. Veal and D.J. Lam, Phys. Rev. B **10**, 4902 (1974) and Phys. Letters **49A**, 466 (1974).
30. S.R. Mishra, T.R. Cummins, G. D. Waddill, W.J. Gammon, G. van der Laan, K.W. Goodman, and J.G. Tobin, Phys. Rev. Lett. **81**, 1306 (1998).
31. Emiliana Damian, "X-ray Emission Spectroscopy Applied in materials Science," Uppsala University, Uppsala, Sweden.
32. L. Duda, http://homepage.mac.com/lcduda/RIPES1.html
33. P.A. Dowben, Surface Science Reports **40**, 151 (2000).

Observation of Strong Resonant Behavior in the Inverse Photoelectron Spectroscopy of Ce Oxide

Figure captions

Figure 1

The XES and RIPES of Ce Oxide is shown here.

Figure 2

Schematic models for the processes of XES and RIPES are illustrated here.

Figure 3

The XES of the Ce 3d states is plotted here.

Figure 4

The XES of the O1s is shown here.

Figure 5

A plot of both the XES and RIPES near the Ce $3d_{5/2}$ threshold is shown here.

Figure 6

A plot of both the XES and RIPES near the Ce $3d_{3/2}$ threshold is shown here.

Figure 7

Here is shown the photon energy dependence of the Ce $3d_{5/2}$ IPES resonance.

Figure 8

Here is shown the photon energy dependence of the Ce $3d_{3/2}$ IPES resonance.

Figure 9

The RIPES and XES of Ce metal is shown here. [32,33]

Observation of Strong Resonant Behavior in the Inverse Photoelectron Spectroscopy of Ce Oxide

Figure 1

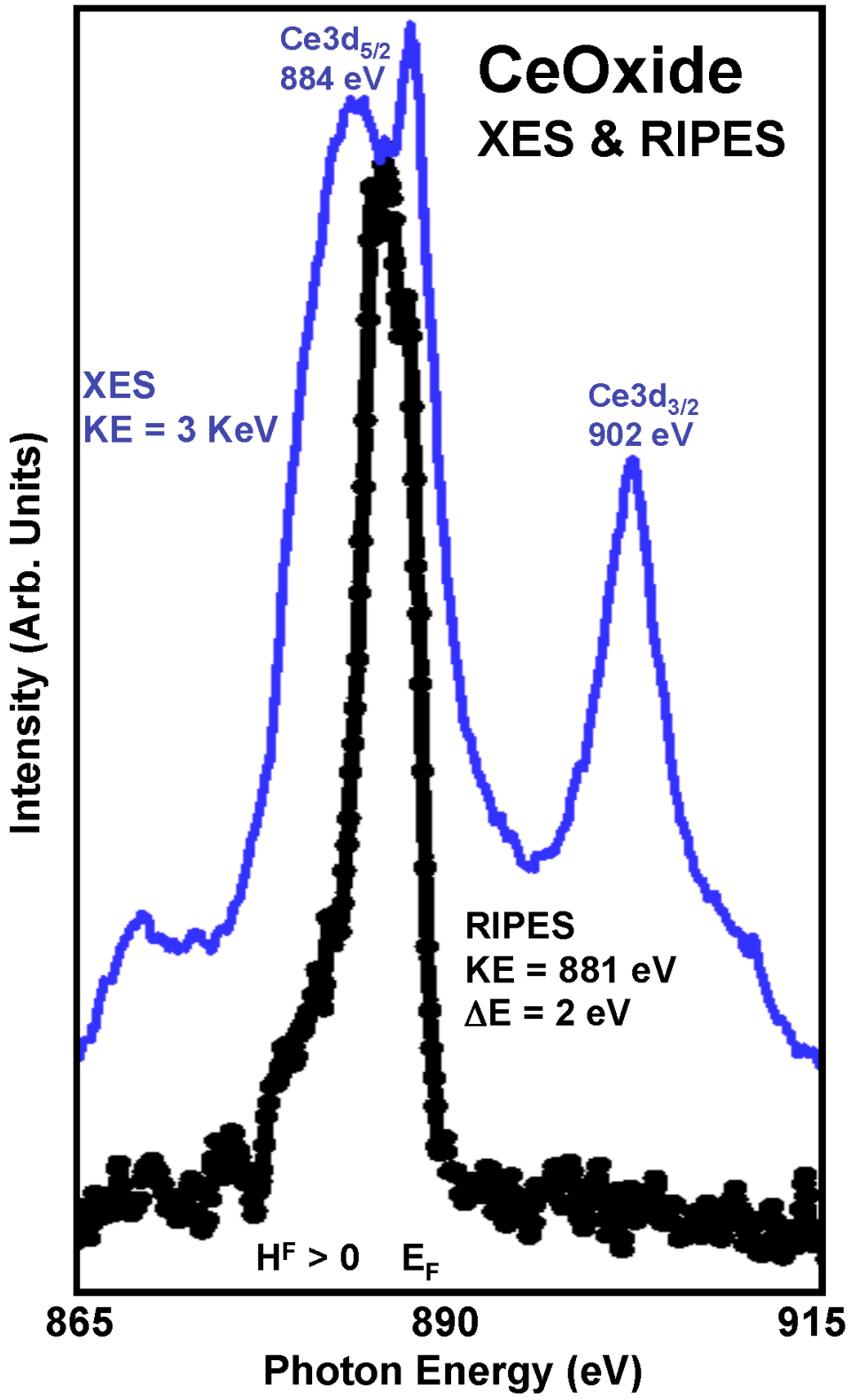

Observation of Strong Resonant Behavior in the Inverse Photoelectron Spectroscopy of Ce Oxide

Figure 2

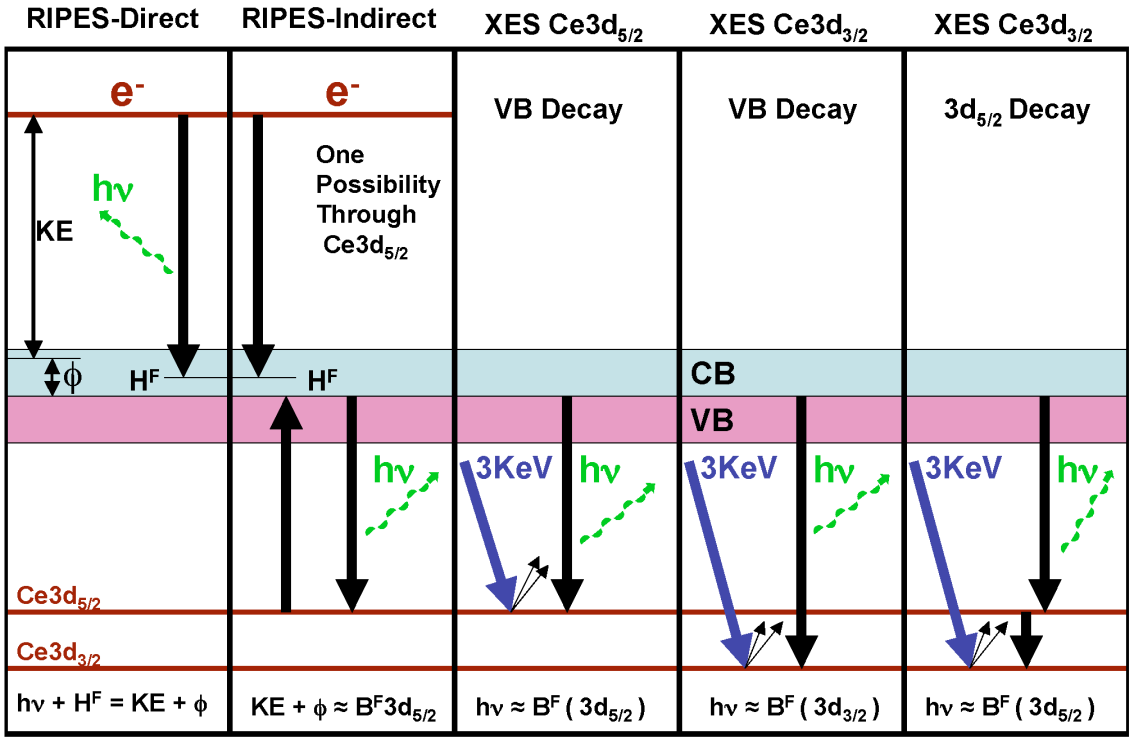

Observation of Strong Resonant Behavior in the Inverse Photoelectron Spectroscopy of Ce Oxide

Figure 3

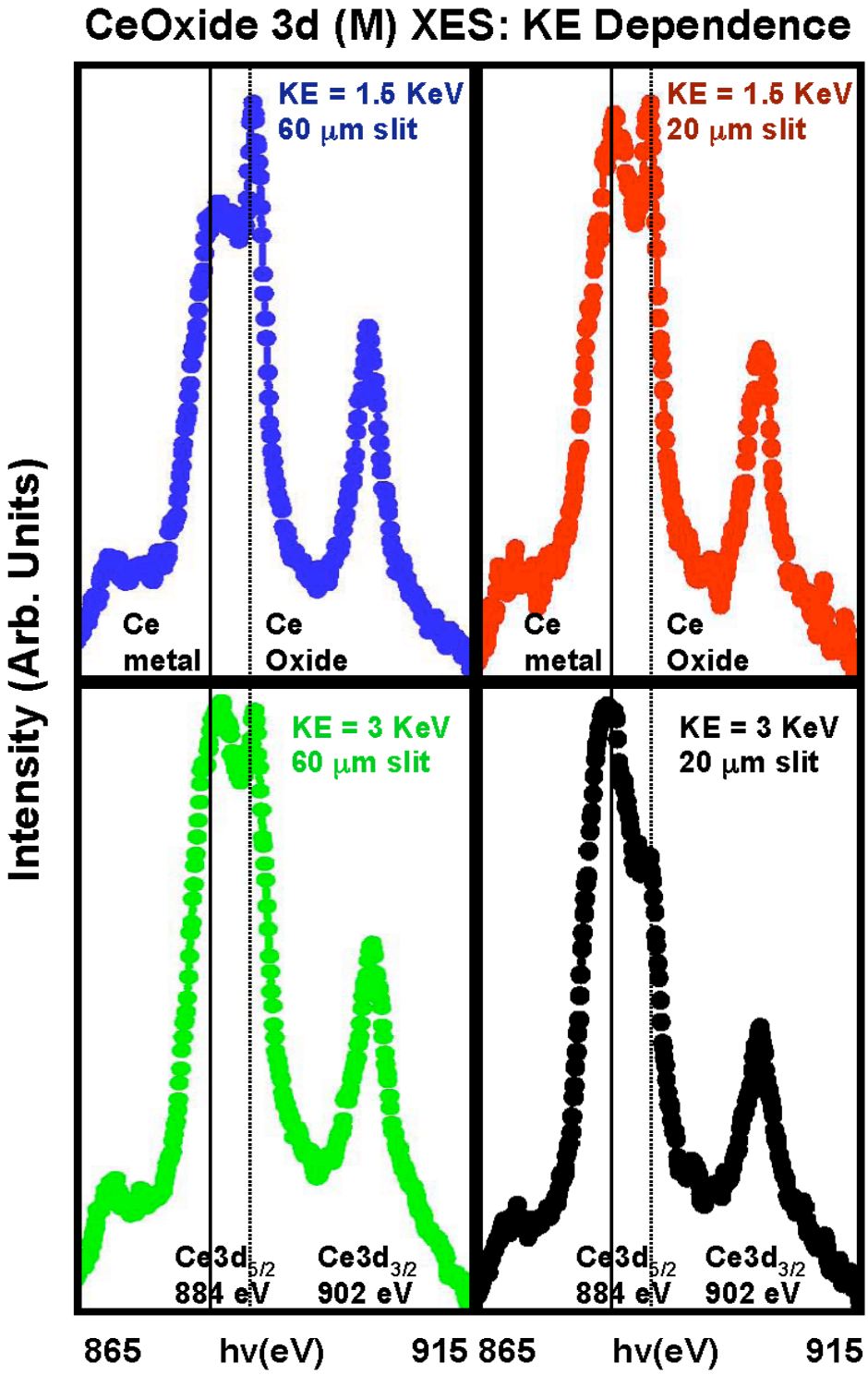

Observation of Strong Resonant Behavior in the Inverse Photoelectron Spectroscopy of Ce Oxide

Figure 4

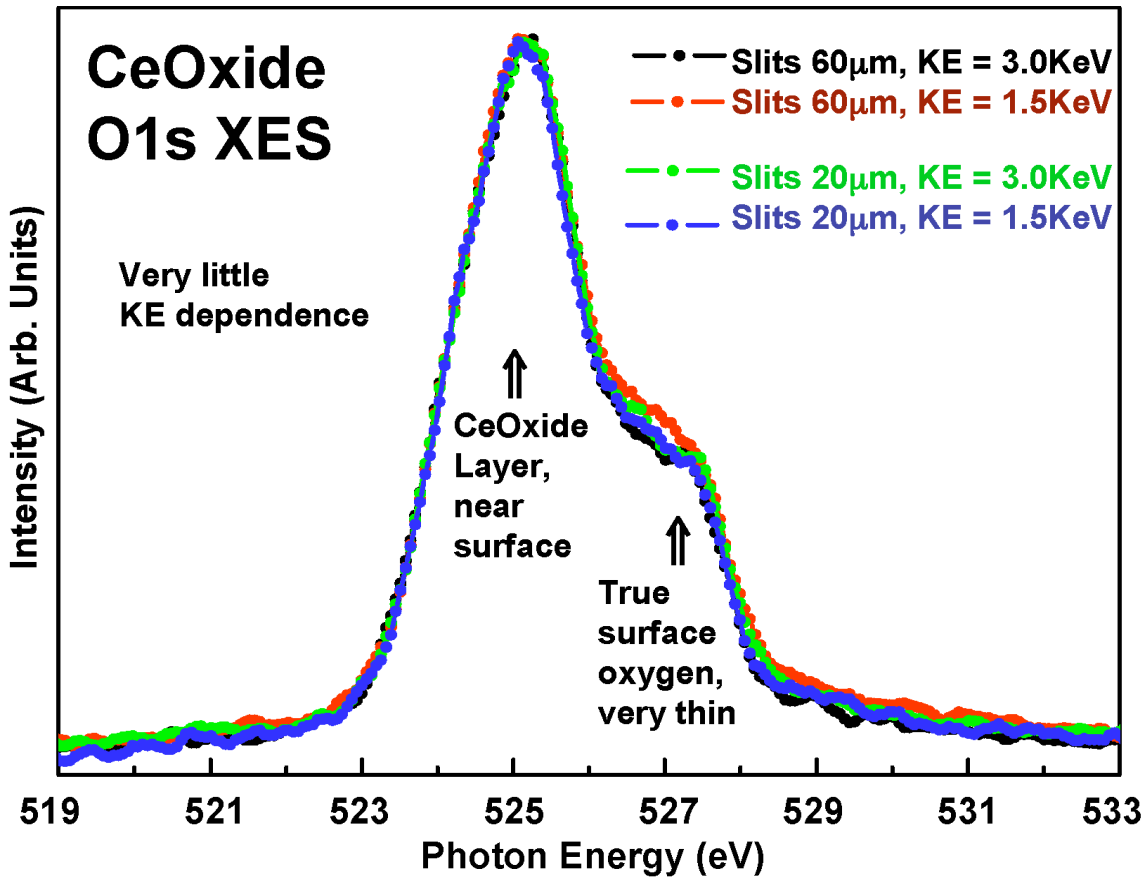

Observation of Strong Resonant Behavior in the Inverse Photoelectron Spectroscopy of Ce Oxide

Figure 5

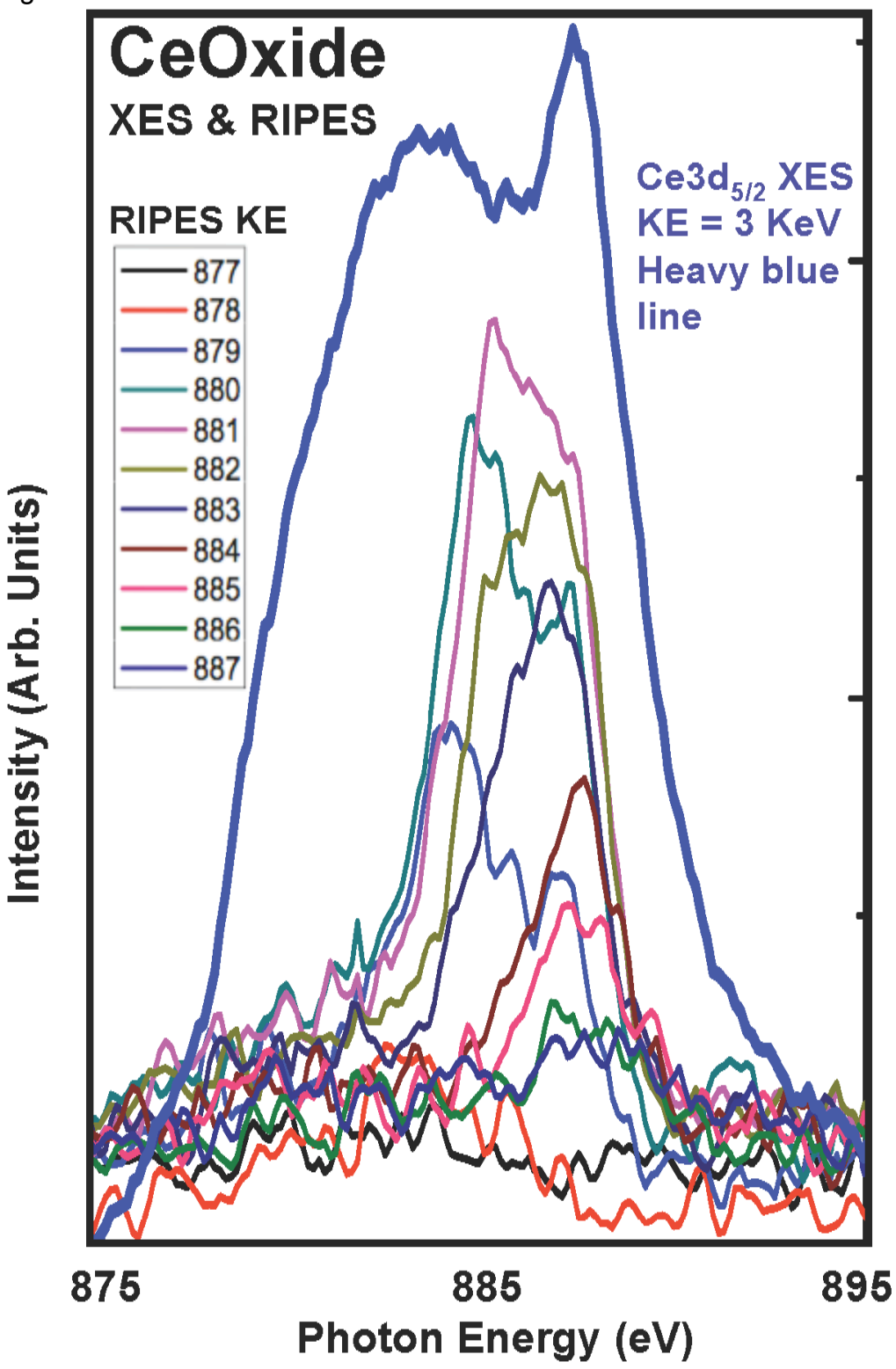

Observation of Strong Resonant Behavior in the Inverse Photoelectron Spectroscopy of Ce Oxide

Figure 6

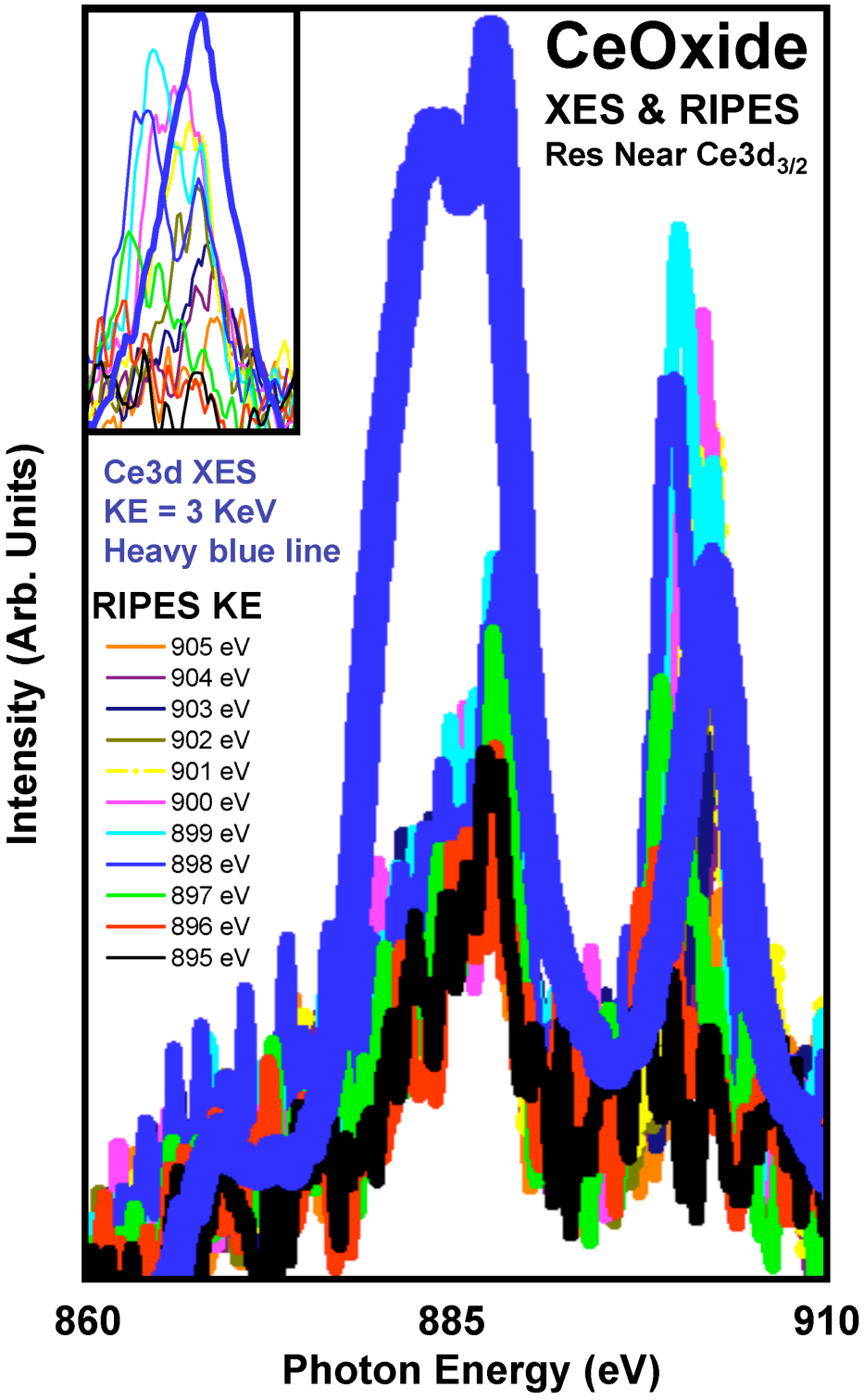

Observation of Strong Resonant Behavior in the Inverse Photoelectron Spectroscopy of Ce Oxide

Figure 7

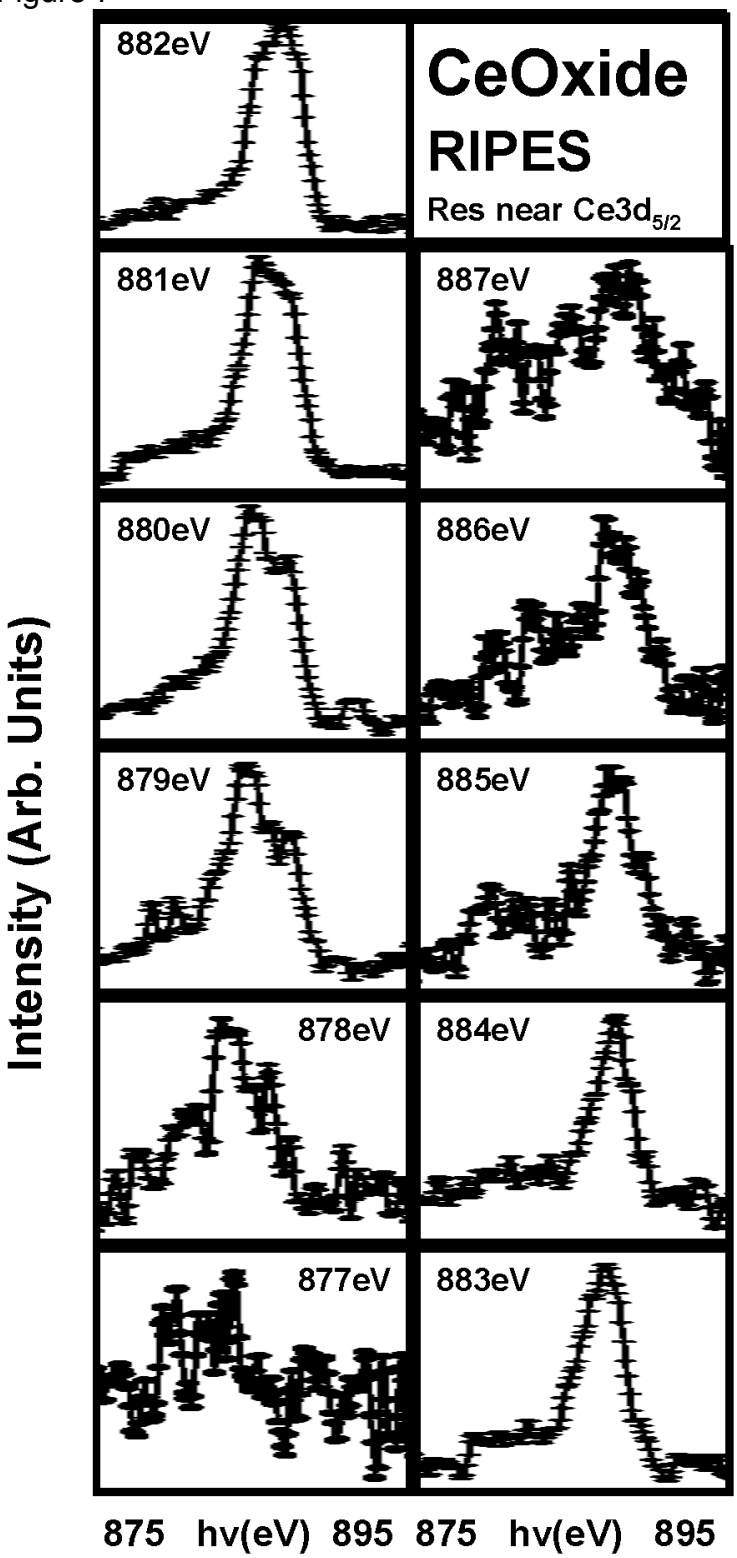

Observation of Strong Resonant Behavior in the Inverse Photoelectron Spectroscopy of Ce Oxide

Figure 8

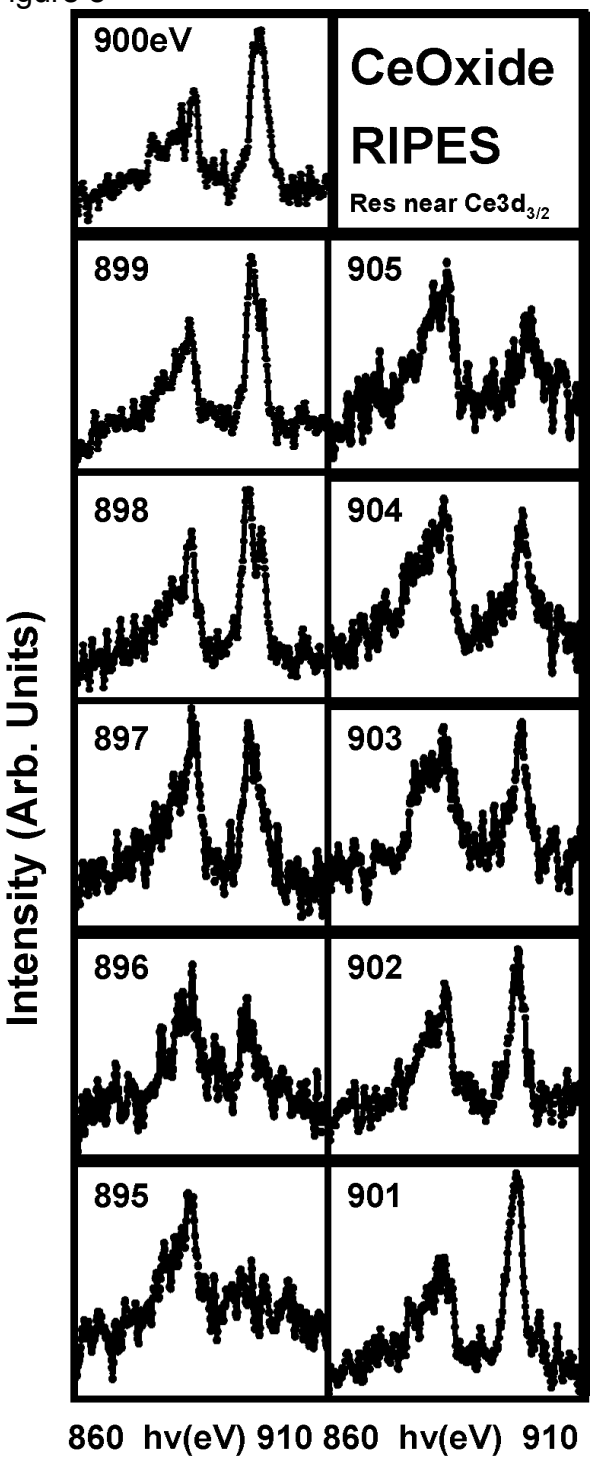

Observation of Strong Resonant Behavior in the Inverse Photoelectron Spectroscopy of Ce Oxide

Figure 9